Nuclear Instruments and Methods in Physics Research B 380 (2016) 76–83

Contents lists available at ScienceDirect

Nuclear Instruments and Methods in Physics Research B

journal homepage: www.elsevier.com/locate/nimb

Electrical properties of as-grown and proton-irradiated high purity silicon

Jerzy Krupka [a,*], Waldemar Karcz [b], Paweł Kamiński [c], Leif Jensen [d]

[a] Institute of Microelectronics and Optoelectronics, Warsaw University of Technology, Koszykowa 75, 00-662 Warsaw, Poland
[b] Joint Institute for Nuclear Research, Joliot-Curie 6, 141980 Dubna, Russia
[c] Institute of Electronic Materials Technology, Wólczyńska 13, 301-919 Warsaw, Poland
[d] Topsil Semiconductor Materials A/S, Siliciumvej 1, DK-3600 Frederikssund, Denmark

ARTICLE INFO

Article history:
Received 9 April 2016
Received in revised form 5 May 2016
Accepted 5 May 2016
Available online 14 May 2016

Keywords:
Silicon
Resistivity
Radiation damage

ABSTRACT

The complex permittivity of as-grown and proton-irradiated samples of high purity silicon obtained by the floating zone method was measured as a function of temperature at a few frequencies in microwave spectrum by employing the quasi TE_{011} and whispering gallery modes excited in the samples under test. The resistivity of the samples was determined from the measured imaginary part of the permittivity. The resistivity was additionally measured at RF frequencies employing capacitive spectroscopy as well as in a standard direct current experiment. The sample of as-grown material had the resistivity of ~85 kΩ cm at room temperature. The sample irradiated with 23-MeV protons had the resistivity of ~500 kΩ cm at 295 K and its behavior was typical of the intrinsic material at room and at elevated temperatures. For the irradiated sample, the extrinsic conductivity region is missing and at temperatures below 250 K hopping conductivity occurs. Thermal cycle hysteresis of the resistivity for the sample of as-grown material is observed. After heating and subsequent cooling of the sample, its resistivity decreases and then slowly (~50 h) returns to the initial value.

1. Introduction

The electrical properties of silicon irradiated with high-energy particles, such as protons, significantly change due to the damage of its crystal lattice [1,2] and such material exhibits extremely high resistivity. Many experimental techniques [3–8] have been used to study the electrical properties of silicon after irradiation. These techniques include Hall effect measurements [9,10], photo-induced current transient spectroscopy [11,12], the pocket pumping method [13] and the microwave split post dielectric resonator method [14]. Studies of irradiation-induced defects in silicon have been also carried out by deep level transient spectroscopy (DLTS), electron paramagnetic resonance (EPR), Fourier transform infrared absorption (FTIR), and photoluminescence spectroscopy (PL). The properties of radiation defect centers determined from these studies were reported e.g. in the references [14–21]. The high resistivity of irradiated silicon is usually explained by the free charge carrier compensation resulting from the appearance of deep energy level centers related to the irradiation defects. The oxygen-related shallow donors were observed earlier in silicon grown by floating zone (FZ) and Czochralski (Cz) techniques, as well as in epitaxial silicon subjected to irradiation with a high fluence of high-energy particles [22,25]. The activation energies of these centers determined from the high-resolution photo induced transient spectroscopy (HRPITS) studies were in the range from 10 to 30 meV. It is believed that irradiation-induced shallow donor centers are associated with electrically active small aggregates of oxygen atoms that are formed during irradiation [22–25]. The diffusivity of oxygen strongly depends on the concentrations of irradiation-induced point defects in silicon [26,27]. The well-known oxygen-related thermal donors that are formed in Czochralski grown silicon by its annealing at 450 C are also identified as oxygen aggregates [28]. Because the native point defect concentrations in an as-grown single crystal are by orders of magnitude lower than those that are formed in an irradiated material, a higher temperature is needed to make the diffusivity of oxygen atoms sufficient for the formation of these aggregates [26,27]. The difference in the electronic properties of the thermal donors results from the different size of the oxygen aggregates.

Detailed studies of the electrical properties of irradiated silicon are important for two reasons. Firstly, high-resistivity silicon detectors are commonly used in nuclear power stations and particle colliders and their properties deteriorate after irradiation, so it

* Corresponding author.
E-mail address: krupka@imio.pw.edu.pl (J. Krupka).

http://dx.doi.org/10.1016/j.nimb.2016.05.007
0168-583X/

is essential to improve their performance. Secondly, after the irradiation with high fluences of high-energy particles, the resistivity of lightly doped silicon becomes very high and such material can find applications in microwave and terahertz technology.

In this work we have performed comparative studies of the electrical properties of the highest purity as-grown and proton-irradiated floating zone silicon as a function of temperature. The major measurement technique which has been used was the contactless dielectric resonator technique which allowed us to measure permittivity and the total dielectric loss tangent of the two kinds of high purity silicon samples. The bulk resistivity of the samples was determined from the measured dielectric loss tangent values. Additionally, the resistivity of the irradiated sample was measured versus temperature by employing standard direct current experiment, at room temperature, by means of capacitive spectroscopy at RF frequencies.

2. Theory

Electromagnetic properties of a semiconductor are specified by the complex relative permittivity (1)

$$\varepsilon_r = \varepsilon_r' - j\varepsilon_r'' - j\frac{1}{\rho\omega\varepsilon_0}, \tag{1}$$

where

ε_0 is the permittivity of vacuum,
ε_r – the relative complex permittivity,
ε_r' – the real part of the relative complex permittivity,
ε_r'' – the imaginary part of the relative complex permittivity,
ω – the angular frequency,
ρ – resistivity.

The imaginary part of the permittivity contains two terms. The first one is associated with dielectric loss mechanisms and the second one with the material conductivity. The dielectric loss tangent is given by the formula

$$\tan\delta = \frac{\mathrm{Im}(\varepsilon_r)}{\mathrm{Re}(\varepsilon_r)} = \tan\delta_d + \frac{1}{\rho\omega\varepsilon_0\varepsilon_r'}, \tag{2}$$

where $\tan\delta_d = \varepsilon_r''/\varepsilon_r'$ denotes dielectric loss tangent associated with pure dielectric loss mechanisms (e.g. electronic and ionic polarization).

We have used both the quasi TE_{011} and the whispering gallery modes to measure each of our samples at a few frequency points. The electric energy filling factors p_e in the samples under test were larger than 0.91 for the whispering gallery modes and about 0.9 for the TE_{011} mode. For the whispering gallery modes the total measured Q-factor values Q_u were practically not affected by the conductor losses in the metal walls of the cavity. Therefore for these modes the dielectric loss tangent was determined from the formula $\tan\delta = 1/(p_e Q_u)$. Such a method was previously used to measure resistivity of gallium arsenide and gallium phosphide [29]. In our earlier paper [30], quasi TE_{011} mode was used for measurements of high resistivity silicon, however its sensitivity is not sufficient to accurately measure the dielectric loss tangent values that are smaller than 1×10^{-5}. Whispering gallery modes allow measurements of arbitrarily small losses and employing them dielectric loss tangent values that were smaller than 1×10^{-9} were measured on sapphire [31].

A schematic of the microwave cavity containing the sample under test is presented in Fig. 1a. The sample under test was situated on a small single crystal quartz support inside a cylindrical cavity and the whole structure was mounted on the cold head of a closed cycle cryo-cooler for low and elevated-temperature measurements.

Additional measurements of the samples at room temperature have been performed in a capacitance dielectric test fixture (Fig. 1b) employing a multilayer model of the sample. In this model it is assumed that the sample under test consists of several layers having different thicknesses and resistivities. The capacitance and the Q-factor of the fixture containing the sample are measured over several decades of frequency. The thickness and resistivity of individual layers are obtained by applying optimization procedure which allows us to achieve the best fit of the model to the experimental data. Details of the measurement procedure are described in [32]. For the irradiated sample we have also performed resistivity measurements using a direct current setup which is depicted in Fig. 1c.

3. Experiments and discussion

Two high resistivity silicon samples were measured. The first one had diameter 13.28 mm and thickness 1.95 mm and the second, irradiated sample, had diameter 13.32 mm and thickness 2.052 mm. The first sample was made from the highest purity silicon obtained by the floating zone method by Topsil Semiconductor Materials A/S. The level of unintentional impurities (Phosphorus, Boron) in this material was smaller than $1\times10^{11}\,\mathrm{cm}^{-3}$ according to the information obtained from the manufacturer. On this sample majority conduction species were not able to be inferred using the available apparatus.

The second sample, also obtained by the floating zone method had a resistivity of 2000 Ω cm before irradiation. The semi-insulating properties of the sample were achieved by its irradiation with 23-MeV protons at the Karlsruhe Institute of Technology. The applied proton fluence was $5\times10^{14}\ n_{eq}/\mathrm{cm}^2$.

Initial information on the electrical properties of both samples was obtained from measurements of the capacitance and Q-factor of the samples versus frequency in the capacitive dielectric test fixture (Fig. 1b). Assuming a 5 layer model of the sample and applying the optimization procedure we have obtained thickness and resistivity of subsequent layers [32]. Results are presented in Table 1. From results that are shown in Table 1 it is seen that the resistivity of the sample is not uniform in the direction perpendicular to the sample surfaces. For the first sample, further denoted as FZ85, the average resistivity is about 85 kΩ cm, while for the second – the irradiated sample, the average resistivity is about 520 kΩ cm at room temperature. The sequence of the layers cannot be determined with the capacitance technique but we suspect that the high resistivity layers correspond to the depletion regions in the vicinity of the surfaces of the samples. It is seen that for the irradiated sample the lowest resistivity fraction (504 kΩ cm) occupies 90% of the volume of the sample. For the FZ85 sample the lowest resistivity fraction (71 kΩ cm) occupies 70% of the volume of the sample (see Fig. 2).

The next experiments have been performed at microwave frequencies in the temperature range from 13 K to 365 K. The resonance frequencies and the unloaded Q-factors of a few different modes were measured as a function of temperature after cooling the fixture to the minimum achievable temperature of 13 K. Measurement results for the first sample at the temperatures of 13 K and 295 K are shown in Table 2.

As has been already mentioned for whispering gallery modes the total dielectric loss tangent can be obtained as $\tan\delta = 1/(p_e Q_u)$ while for the quasi TE_{011} mode the Q-factor due to conductor losses in metal cavity walls must be taken into account to determine the Q-factor Q_S depending on the losses in the sample and then the total dielectric loss tangent. In practice we have used appropriate software dedicated to determination of permittivity and the dielectric loss tangent in the quasi TE_{011}

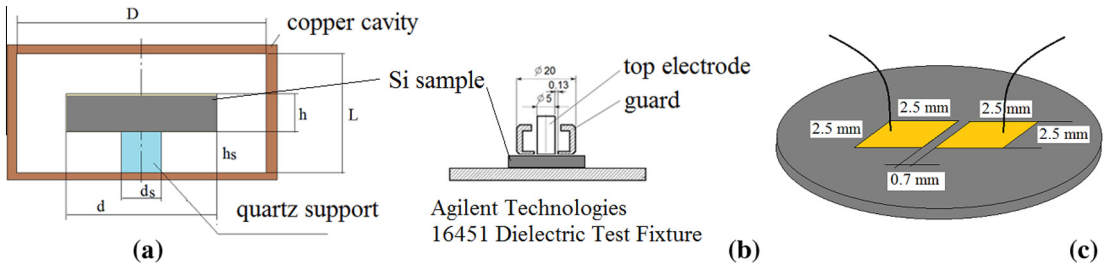

Fig. 1. (a) Sketch of dielectric resonator created by the sample under test, (b) capacitance dielectric test fixture and (c) DC experiment setup.

Table 1
Resistivity and thickness of layers in five layer models of the FZ85 and the irradiated samples.

FZ 85 kΩ cm		Irradiated	
h (μm)	ρ (Ω cm)	h (μm)	ρ (Ω cm)
26.0	1.310E+10	113.0	5.422E+09
76.1	6.042E+07	9.3	3.426E+08
152.7	2.198E+06	18.1	4.102E+07
329.8	2.995E+05	47.1	1.224E+07
1365.3	7.112E+04	1864.5	5.044E+05

cavity. At room temperatures the part of the dielectric loss tangent of silicon depending on pure dielectric losses is equal to 1.2×10^{-5} in the whole microwave frequency spectrum [33], so we have subtracted this value from the total dielectric loss tangent to determine the part associated with conductor losses, at temperatures from 280 to 330 K. At cryogenic temperatures the dielectric tangent value depending on pure dielectric losses for silicon is unknown. In principle it can be determined from measurement results at different frequencies at fixed temperatures. As is shown in Table 2 the Q-factor values measured at 13 K increase with frequency in a similar manner as at 295 K, so the assumption that the loss tangent measured at 13 K predominantly depends on the conductor losses is reasonable.

The results of permittivity and the total dielectric loss tangent determination for the irradiated sample as a function of temperature are shown in Fig. 3a and b. The permittivity values of both the sample of as-grown material and the irradiated sample are essentially the same in the range of measurement uncertainties. However, the values of dielectric loss tangents and the resistivity for the two kinds of samples behave in completely different manners. The graphs showing the determined results of resistivity for the two kinds of samples are presented in Fig. 4. For comparison, the results of our measurements on the sample having room temperature resistivity of 13 kΩ cm are presented. Additional DC measurements have been performed on a small irradiated sample by depositing two square gold contacts (2.5 mm × 2.5 mm) on its surface, separated by a 0.7 mm distance. Because the distance between the contacts was much smaller than the width of the gold squares we have assumed that the sheet resistance of the sample is equal to the measured resistance value.

Four temperature regions are clearly seen for the samples of as-grown FZ silicon: namely the intrinsic range, the extrinsic range, freeze-out range, and the low temperature range. For the irradiated sample the extrinsic range is missing. The resistivity in the extrinsic range for the samples of as-grown material increases with the temperature because the mobility of charge carriers decreases with increasing temperature and the free charge carrier concentration in this range is constant. For the irradiated sample the free charge carriers are trapped by deep energy level centers introduced by irradiation.

Let us analyze our experimental results in detail taking into account literature data [34–45]. To do that, firstly we have to make assumptions on the temperature dependence of the forbidden energy gap and on the intrinsic carrier concentration. We have assumed the following, commonly cited [34], expression for the forbidden gap energy dependence on temperature:

$$E_g = 1.1785 - 9.025 \times 10^{-5} \times T - 3.05 \times 10^{-7} \times T^2. \quad (3)$$

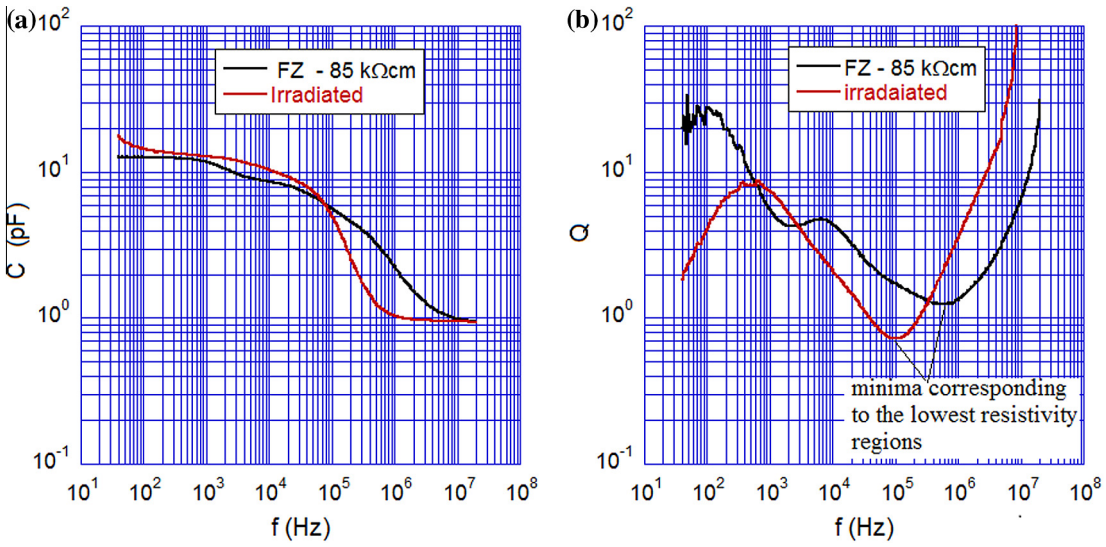

Fig. 2. Results of room temperature (295 K) measurements of (a) capacitance and (b) Q-factor versus frequency for the FZ85 and the irradiated silicon samples.

Table 2
The resonance frequencies, the unloaded Q-factors, and the electric energy filling factors of three modes that were employed in measurements of the FZ85 sample.

Mode	p_e	T = 13 K		T = 295 K	
		f (MHz)	Q_u	f (MHz)	Q_u
S2-9	0.957	39,752	188,000	39,437	17,615
S1-5	0.915	22,613	105,000	22,449	10,027
Quasi TE011	0.899	10,731	39,407*	10,641	4880

* Q_S = 64,600 (Q-factor due to the losses in the sample).

It is worth adding that there is a range of data in the literature [35–38] on the value of the intrinsic carrier concentration of silicon at 300 K. There are two alternative values of $n_i(300)$ in literature [35,36] that well agree with the best existing experimental data namely: $n_i(300) = 9.72 \times 10^9$ cm^{-3} and $n_i(300) = 1.08 \times 10^{10}$ cm^{-3}. In the further analysis of experimental data we assume the following expression for the temperature dependence of the intrinsic carriers concentration, with the two alternate values of $n_i(300)$:

$$n_i = C(300) \times T_n^{3/2} \exp\left(-\frac{E_g}{2k_B T}\right), \tag{4}$$

where $C(300) = n_i(300)/\exp\left(-\frac{E_g(300)}{600k_B}\right)$, $T_n = T/300$, and k_B is the Boltzmann constant.

In Fig. 5, the resistivity of both the as-grown (FZ85) and irradiated samples as a function of $(2k_BT)^{-1}$ is presented in the intrinsic range of temperatures. It is seen that all experimental points for the irradiated sample are situated exactly on the straight line with the slope of 1.13 eV. The slope agrees within 1% uncertainty with the forbidden energy gap of silicon at 300 K. The asymptotic value of the slope for the FZ85 sample is equal to the forbidden energy gap of silicon at 300 K. Assuming that for the irradiated sample's free charge carriers, the numbers of electrons and holes are the same and equal to n_i given by formulae (4), one can determine the sum of the electron and hole mobilities $\mu_{eff} = (\mu_e + \mu_h)$ from the formula $(\mu_e + \mu_h) = (q_e \rho n_i)^{-1}$ [37]. In Table 3, the results evaluated from the experimental data are presented for the two assumed values of intrinsic carrier concentrations at 300 K and the formulae (4) for their temperature dependance.

The results that are shown in Table 3 are in excellent agreement with the literature, although the literature data are usually [39] based on the mobility measurements for silicon samples with one dominant charge carrier and with much higher charge carrier concentrations.

For the FZ85 sample, the determination of the effective mobility of charge carriers is not straightforward. One has to assume at least two additional parameters for its evaluation. The first one is the ratio of the mobility of electrons to the mobility of holes. The second one is the net charge associated with the ionized impurities i.e. $N_D^+ - N_A^-$. We have assumed $\mu_e = 3\mu_h$. The concentration of free charge carriers in a doped semiconductor can be evaluated from the charge neutrality condition. For the n-type semiconductor, when $N_D^+ > N_A^-$, the formulae for the charge carrier concentrations can be written as follows

$$n = \frac{N_D^+ - N_A^-}{2} + \left(\left(\frac{N_D^+ - N_A^-}{2}\right)^2 + n_i^2\right)^{1/2} \quad p = n_i^2/n \tag{5}$$

while for the p-type semiconductor it reads as

$$p = \frac{N_A^- - N_D^+}{2} + \left(\left(\frac{N_A^- - N_D^+}{2}\right)^2 + n_i^2\right)^{1/2} \quad n = n_i^2/p. \tag{6}$$

Taking into account formulae (5), (6) and assuming that the assumption $\mu_e = 3\mu_h$ holds in the extrinsic and the intrinsic temperature ranges, it is possible to assess the temperature dependence of the electron mobility, the hole mobility, and the effective mobility from the measured values of resistivity for a given value of the uncompensated charge concentrations: $N_D^+ - N_A^-$. E.g. the mobility of electrons for the n-type semiconductor was evaluated as $\mu_e = (q\rho(n + p/3)^{-1})$ with a concentration of electrons and holes given by (5). The results of our numerical experiments are shown in Fig. 6. In the low temperature region the effective mobility curves overlap under the assumption that concentration uncompensated donors in a n-type semiconductor is 3 times larger than the concentration of uncompensated acceptors in a p-type semiconductor. This is a consequence of the assumption that the mobility of electrons is 3 times larger than the mobility of holes. The solid curve represents a simple power function fit to the experimental data taking into account only the FZ85 results for temperatures below 200 K and the irradiated sample results. The effective mobility values determined from the experiments for the FZ85 sample are closer to the fitting function,

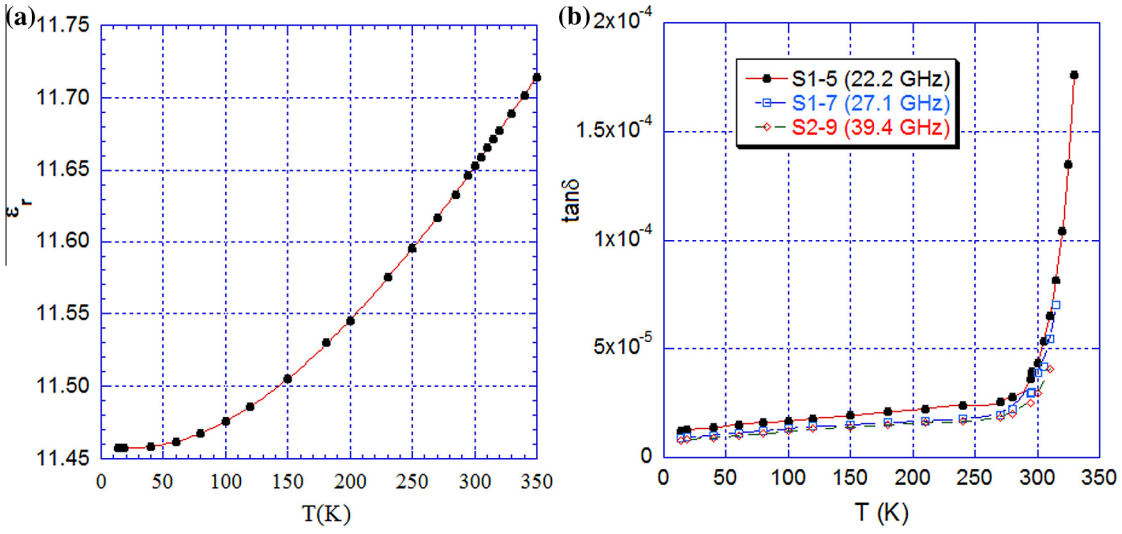

Fig. 3. (a) Temperature dependence of permittivity for both FZ85 and irradiated samples. (b) The total dielectric loss tangent for the irradiated sample versus temperature at various microwave frequencies.

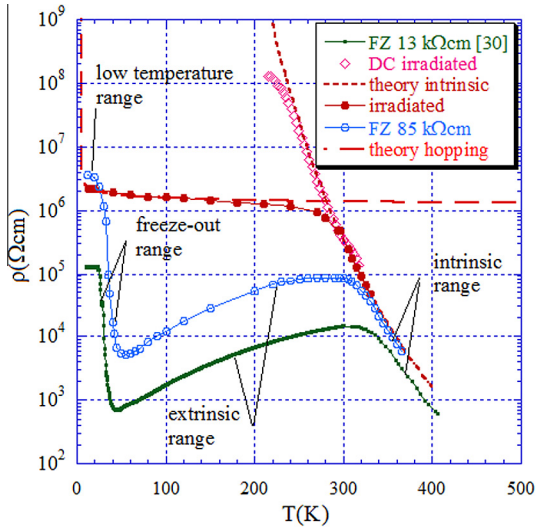

Fig. 4. Resistivity of the as-grown (FZ85) and irradiated silicon samples versus temperature, determined from microwave measurements. The irradiated sample was additionally measured with the DC method. Results of our old measurements [30] for the other as-grown silicon (FZ13) sample with the room temperature resistivity of 13 kΩ cm are presented for comparison.

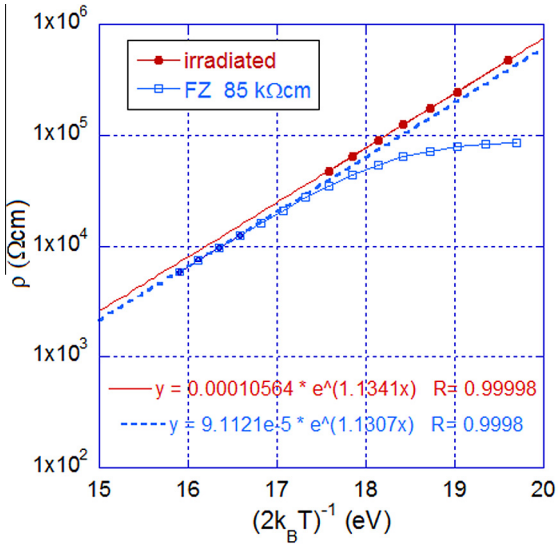

Fig. 5. Resistivity of the as-grown (FZ85) and irradiated silicon samples in the intrinsic range determined from microwave measurements.

Table 3
Sum of the electron and hole mobility values at the intrinsic region determined from resistivity measurements on the irradiated sample.

T (K)	$(\mu_e + \mu_h)$ for $n_i(300) = 1.08 \times 10^{10}$	$(\mu_e + \mu_h)$ for $n_i(300) = 9.72 \times 10^{9}$
296.0	1704	1893
305.0	1549	1722
310.0	1471	1633
315.0	1413	1570
320.0	1344	1493
325.0	1298	1442
330.0	1244	1383

at the temperature range from 300 K to 350 K, for the assumption that the semiconductor is n-type in this range. But even for the n-type assumption the effective mobility dependence on the

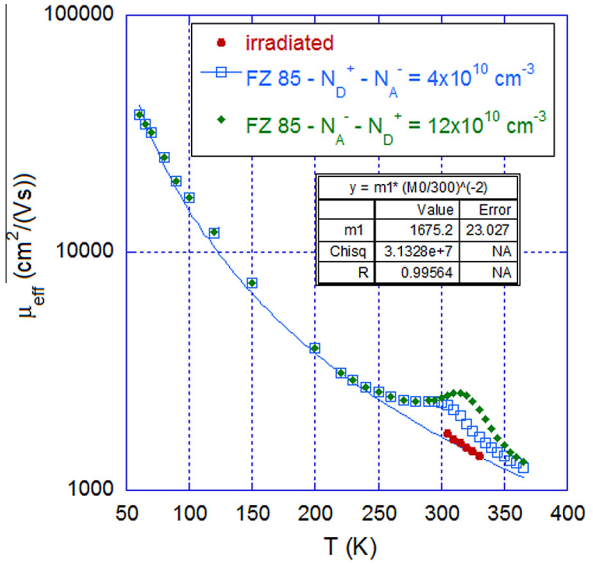

Fig. 6. The effective mobility of charge carriers in the as-grown (FZ85) and irradiated silicon samples as a function of temperature.

temperature for the FZ85 sample exhibits a local maximum at the temperature range from 250 K to 350 K. The effective mobility of the irradiated sample in this temperature range monotonically decreases, as was also shown in Table 3. An explanation of such behavior for the FZ85 sample is that the number of free charge carriers in this temperature range is larger than was determined from formulas (5) and (6), while the effective mobility of charge carriers follows the fitting curve.

One of the reasons for that would be free charge emission/capture processes. The rate of thermal emission of free charge carriers is fast, while the process of their capture is much slower. Variations of the free carrier concentrations with respect to the theoretical predictions can be related to the presence and influence of deep donor and/or acceptor impurities that would trap or release free charge carriers at different rates at different temperatures. Such a phenomenon was observed while performing cyclic measurements of the resistivity versus temperature. The results of this experiment are presented in Fig. 7. When the sample is cooled down to the lowest temperature (about 13 K in our case) and then the temperature is raised, the variations of the resistivity versus temperature look like in Fig. 4. When one performs the measurements in a temperature cycle, the results look like in Fig. 7. When the sample is initially cooled down and then heated up, the resistivity values are very similar at a fixed temperature on different parts of the thermal cycle (parts I and II in Fig. 7).

When the sample is initially heated up and then cooled down the differences between resistivity values, measured at the same temperature but at different parts of the thermal cycle, are significant (parts II and III in Fig. 7). The resistivity recovers to the initial value after leaving the sample at room temperature for about 48 h. The observed thermal hysteresis is probably related to the slow processes of charge carrier capture by deep donor and/or acceptor defect centers, the same that were responsible for the increase of the free charge carrier concentration that was observed in Fig. 6. As it was shown in [14] the concentration of the deep defect centers in the irradiated silicon is relatively small $\sim 10^{15}$ cm^{-3} so the probability that thermally generated free charge carriers are trapped after cooling the sample is also small. This takes a time so equilibrium is achieved after several hours.

Finally we will analyze in detail results of resistivity in the low temperature range. In Fig. 8, the resistivity values of the FZ13 and

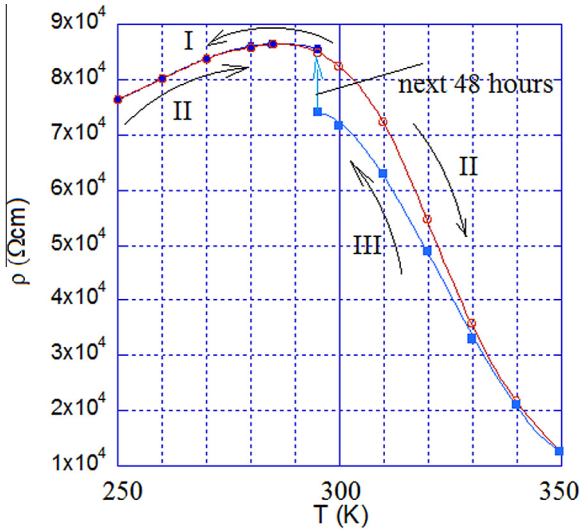

Fig. 7. Hysteresis due to thermal cycling of silicon in resistivity measurements for the sample of as-grown material (FZ85). The sample is first cooled down from 295 K to 250 K (I) then heated up from 250 K to 350 K (II) and finally cooled down from 350 K to 295 K (III).

FZ85 samples as well as the resistivity of the irradiated sample are presented as a function of $(2k_BT)^{-1}$. Freeze-out regions are clearly visible for the FZ85 and FZ13 samples. The activation energies of shallow impurities in the FZ13 and FZ85 samples, obtained from the slopes of the curves, are 0.045 eV and 0.0457 eV, respectively, and they are represented in Fig. 8a and b as the fitting parameter m2. The values of the activation energies indicate the presence of boron or phosphorus atoms.

At the lowest temperature range, the resistivity is almost constant for all samples with the lowest value being $10^5\,\Omega$ cm for the FZ13 sample and the highest value being $3.4\times10^6\,\Omega$ cm for the FZ85 sample. The resistivity value for the irradiated sample at 13 K is equal to $2.2\times10^6\,\Omega$ cm and it slowly decreases with increasing temperature. A finite value of the semiconductors resistivity at the lowest temperatures that are not sufficient for ionization of shallow donors and acceptors is called impurity conduction or hopping conduction [40–45]. Because of the Coulomb forces between the ionized impurities, the state of lowest energy is achieved when the majority impurity nearest neighbor (in 3D space) to a given minority impurity is ionized. When a steady electric field is applied, a current can flow only if the thermal energy is sufficient to overcome the Coulomb potential around the minority impurity. If the energy is insufficient, the potential is altered by the applied electric field, and a new equilibrium has to be established. This takes a time, the order of the hopping time, so a net polarization occurs.

Polarization phenomena related to the hopping conductivity can be detected in RF and microwave experiments. Such experiments have been performed by Pollak and Geballe [43] at the frequency range from 100 Hz to 100 kHz and the temperature range from 1 K to 20 K on several silicon samples. The authors have shown that the real part of the measured AC conductivity, which is related to the hopping conductivity mechanisms, increases with frequency according to the formula $\sigma = A\omega^{0.8}$, where A is a complex constant. As a consequence of the frequency dependence, the hopping conductivity is higher at microwave frequencies than at RF frequencies. This was observed in all our samples. Moreover, the hopping conduction in the irradiated sample extends up to the intrinsic region. Additional information and explanation of the hopping conductivity on the foundation of percolation theory can be found in e.g. Shklovskii, A. L. Efros [44], and Shegelski, Barrie [45]. According to theory presented in [45], the DC electrical conductivity of disordered systems where hopping conductivity occurs is characterized by temperature dependence of the resistivity given by

$$\rho = \rho_0 \exp((T_0/T)^{0.25}). \tag{7}$$

Using the experimental data for the irradiated sample in the temperature range from 13 K to 200 K one obtains the following parameters of the model that provide the best least squares fit to the experimental data: $\rho_0 = 8.86\times10^5\,\Omega$ cm, $T_0 = 11.2$ K. In Fig. 4, the results of modeling are presented as the "theory hopping" curve. It is seen that agreement between theory and experiment for the irradiated sample is good, however, it should be noted that measurements at the temperatures that are lower than 13 K would be necessary to confirm validity of that model at temperatures below 10 K.

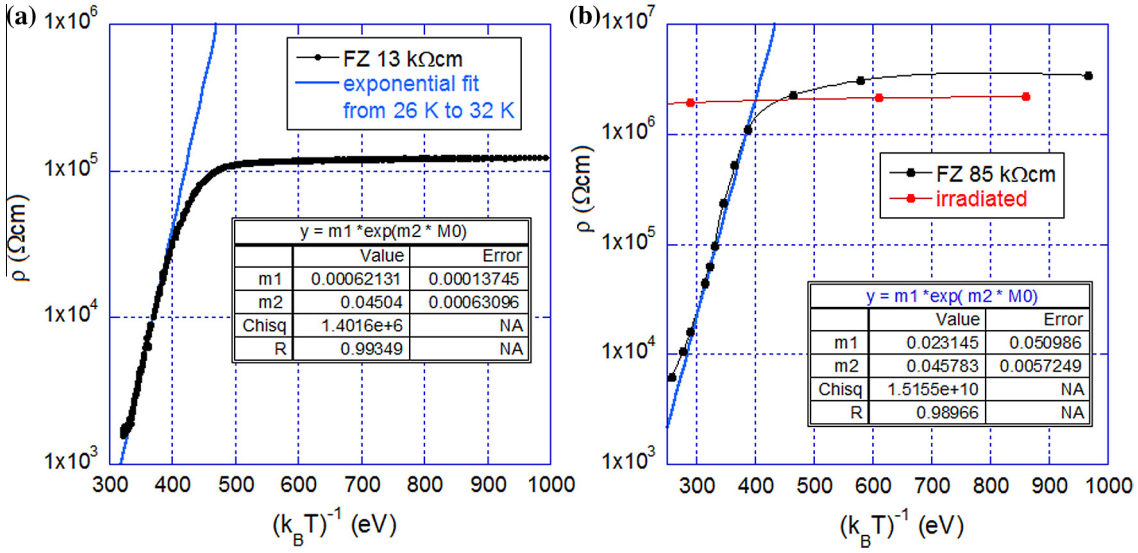

Fig. 8. (a) The resistivity of the 13 kΩ cm FZ silicon sample and (b) the resistivity of the 85 kΩ cm and irradiated FZ – 2 kΩ cm silicon samples as a function of the k_BT reciprocal in the low temperature region.

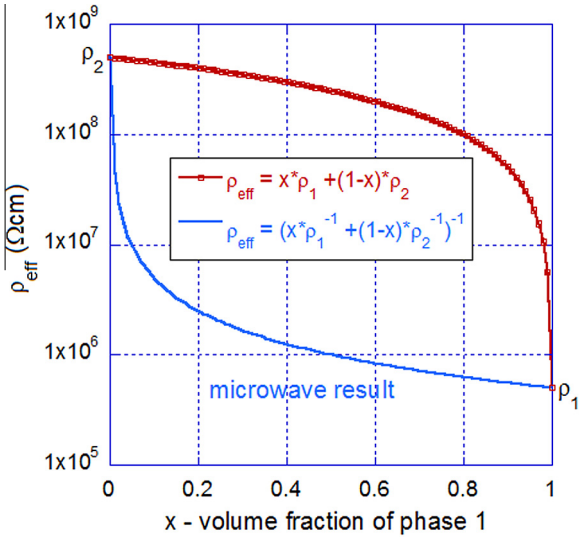

Fig. 9. Boundary curves for the effective resistivity of arbitrary mixtures of two semiconductors with the resistivity $\rho_1 = 5 \times 10^5$ Ω cm and $\rho_2 = 5 \times 10^8$ Ω cm, respectively.

Percolation theory is better supported by microwave experiments than by DC experiments. If a sample contains isolated conductive regions that are immersed in a dielectric medium, the microwave method provides a weighted average value of the total (including conductivity term) losses of the sample. For such a case DC experiment would produce infinite resistivity. To explain how this model works for the irradiated sample, let us assume that the sample consists of two phases with different resistivities. Denote the volume fraction of phase one, having the resistivity of ρ_1, by "x". The volume fraction of the phase two, with the resistivity of ρ_2, will have the volume fraction of $(1 - x)$. It is well known [46] that the effective resistivity of the mixture of two phases is somewhere between the two boundary curves, the first one corresponding to the parallel connection of and the second corresponding to the in series connection of the single phase layers.

In Fig. 9, the boundary resistivity curves are presented for $\rho_1 = 5 \times 10^5$ Ω cm and $\rho_2 = 5 \times 10^8$ Ω cm as a function of the volume fraction of the two phases. The lower boundary curve corresponds to the microwave resistivity measurements. On the other hand, the DC and RF experiments will give the resistivity value for a fixed volume fraction that is somewhere between the two boundary curves. This simple model qualitatively describes the differences between resistivity values measured with microwave, RF and DC methods.

It should be mentioned that the intrinsic properties of irradiated samples last for a long time (several months) if samples are kept at relatively low temperatures (room temperature and below). When such samples are heated up to few hundred degrees Celsius their particular properties (especially high resistivity) disappear, approaching the initial values before irradiation. To avoid degradation of the irradiated sample we have performed measurements at temperatures not exceeding 330 K.

4. Summary

We have compared the temperature dependences of the resistivity of as-grown and proton irradiated high purity FZ silicon measured by the microwave method at temperatures ranging from 13 to 330 K. At the temperature of 295 K, the resistivity of the as-grown material samples was 13 and 85 kΩ cm and that of the proton-irradiated sample was ~500 kΩ cm. At the temperatures above 300 K, the increase in the resistivity of all the samples is due to decreasing the intrinsic concentration of thermally generated electron–hole pairs. The bandgap energy determined at 300 K for the as-grown and irradiated material is 1.13 eV. With increasing material resistivity, the intrinsic conductivity region extends to the lower temperature and for the irradiated material this temperature is 295 K. At temperatures ranging from 295 to 60 K, the conductivity of the as-grown material is controlled either by the concentrations of residual shallow impurities (boron and phosphorus) or the mobility of free charge carriers. The decrease in the resistivity with decreasing temperature is mainly due to the increased mobility of the free charge carriers linked to the decreasing scattering intensity. In this temperature range, the changes in the resistivity of the highly-compensated irradiated material are typical of the hopping mechanism that seems to be significantly enhanced by the microwave radiation.

References

[1] C.J. Bebek, D.E. Groom, S.E. Holland, A. Karcher, W.F. Kolbe, J. Lee, M.E. Levi, N.P. Palaio, B.T. Turko, M.C. Uslenghi, M.T. Wagner, G. Wang, IEEE Trans. Nucl. Sci. 49 (2002) 1221.
[2] J. Janesick, G. Soli, T. Elliot, S. Collins, Proc. SPIE 1447 (1991) 87.
[3] P. Hazdra, K. Brand, J. Vobecky, Nucl. Instr. Meth. B 192 (2002) 291.
[4] S.K. Dubey, A.D. Yadav, B.K. Kamalapurkar, T.K. Gundu Rao, M. Gokhale, T. Mohanty, D. Kanjilal, Nucl. Instr. Meth. B 244 (2006) 157.
[5] M. Jadan, A.R. Chelyadinskii, V.Yu. Yavid, Nucl. Instr. Meth. B 225 (2004) 516.
[6] E. Simoen, C. Claeys, V. Privitera, S. Coffa, M. Kokkoris, E. Kossionides, G. Fanourakis, A. Nylandsted Larsen, P. Clauws, Nucl. Instr. Meth. B 186 (2002) 19.
[7] M. Moll, E. Fretwurst, M. Kuhnke, G. Lindstrom, Nucl. Instr. Meth. Phys. Res., B 186 (2002) 100.
[8] M. Kuhnke, E. Fretwurst, G. Lindstroem, Nucl. Instr. Meth. Phys. Res., B 186 (2002) 144.
[9] D. Konozenko, A.K. Semenyuk, W.I. Khivrich, in: I.W. Corbett, G.D. Watkins (Eds.), Conf. Proc. on Radiation Effects in Semiconductors, Gordon and Breach, 1970.
[10] E. Borchi, M. Bruzzi, B. Dezillie, S. Lazanu, Z. Li, S. Pirollo, IEEE Trans. Nucl. Sci. 46 (1999) 834.
[11] N.T. Bagraev, Semicond. Sci. Technol. 9 (1994) 61.
[12] P.F. Ermolov, D.E. Karmanov, A.K. Leflat, V.M. Manankov, M.M. Merkin, E.K. Shabalina, Semiconductors 36 (2002) 1114.
[13] J. Janesick, Scientific Charge-Coupled Devices, SPIE Press, 2001.
[14] J. Krupka, W. Karcz, S.P. Avdeyev, P. Kaminski, R. Kozlowski, Nucl. Instr. Meth. B 325 (2014) 107.
[15] G.D. Watkins, J.W. Corbett, Phys. Rev. 138 (1965) A543.
[16] R.E. Whan, J. Appl. Phys. 37 (1966) 3378.
[17] Young-Hoon Lee, James W. Corbett, Phys. Rev. B 8 (1973) 2810.
[18] D.V. Lang, J. Appl. Phys. 45 (1974) 3023.
[19] G.D. Watkins, J.R. Troxell, Phys. Rev. Lett. 44 (1980) 593.
[20] B.G. Svensson, B. Mohadjeri, Phys. Rev. B 43 (1991) 2292.
[21] K. Gill, G. Hall, B. MacEvoy, J. Appl. Phys. 82 (1997) 126.
[22] D.J. Chadi, Phys. Rev. B 41 (1990) 10595.
[23] R. Kozłowski, P. Kaminski, E. Nossarzewska-Orłowska, E. Fretwurst, G. Lindstroem, M. Pawłowski, Nucl. Instr. Meth. Phys. Res., A 552 (2005) 71.
[24] Y. Omura, Y. Zohta, M. Kanazawa, Solid State Commun. 11 (1972) 263.
[25] R. Kozłowski, P. Kaminski, E. Nossarzewska-Orłowska, Nucl. Instr. Meth. Phys. Res., A 476 (2002) 639.
[26] V.V. Voronkov, Semicond. Sci. Technol. 8 (1993) 2037.
[27] A.S. Oates, M.J. Binns, R.C. Newman, J.H. Tucker, J.G. Wilkes, A. Wilkinson, J. Phys. C: Solid State Phys. 17 (1984) 5695.
[28] U. Gösele, T.Y. Tan, Appl. Phys. A 28 (1982) 79.
[29] J. Krupka, D. Mouneyrac, J.G. Hartnett, M.E. Tobar, IEEE Trans. Microwave Theory Tech. 56 (2008) 1201.
[30] J. Krupka, J. Breeze, A. Centeno, N. Alford, T. Claussen, L. Jensen, IEEE Trans. Microwave Theory Tech. 54 (2006) 3995.
[31] J. Krupka, K. Derzakowski, A. Abramowicz, M.E. Tobar, R.G. Geyer, IEEE Trans. Microwave Theory Tech. 47 (1999) 752.
[32] J. Krupka, J. Judek, IEEE Trans. Semicond. Manuf. 27 (2014) 530.
[33] J. Krupka, P. Kaminski, R. Kozlowski, B. Surma, A. Dierlam, M. Kwestarz, Appl. Phys. Lett. 107 (2015) 082105.
[34] W. Bludau, A. Onton, W. Heinke, J. Appl. Phys. 45 (1974) 1846.
[35] M.A. Green, J. Appl. Phys. 67 (1990) 2944.
[36] B. Sproul, M.A. Green, J. Appl. Phys. 70 (1991) 846.
[37] S.M. Sze, Physics of Semiconductor Devices, 2nd ed., Wiley, New York, 1981.
[38] H.F. Wolf, Semiconductors, Wiley, New York, 1971.
[39] S. Reggiani, M. Valdinoci, L. Colalongo, M. Rudan, G. Baccarani, A.D. Stricker, F. Illien, N. Felber, W. Fichtner, L. Zullino, IEEE Trans. Electron Dev. 49 (2002) 490.
[40] S. Hung, J.R. Gleissman, Phys. Rev. 79 (1950) 726.
[41] E.M. Conwell, Phys. Rev. 103 (1956) 51.
[42] N.F. Mott, Can. J. Phys. 34 (1956) 1356.

[43] M. Pollak, T.H. Geballe, Phys. Rev. 122 (1961) 1742.
[44] B.I. Shklovskii, A.L. Efros, Electronic Properties of Doped Semiconductors, Springer, Berlin, 1984.
[45] M.R.A. Shegelski, R. Berrie, Phys. Rev. B 36 (1987) 7549.
[46] D.R. Askeland, P.P. Fullay, W.J. Wright (Eds.), The Science and Engineering of Materials, 6th ed., Cengage Learning. Inc., Boston, 2010.